Supplementary Information

Engineering One-Dimensional Hollow beta-In_2S_3/In_2O_3 Hexagonal Micro-Tubes for Efficient Broadband-Light Photocatalytic Performance

Qiuyan Shen,† Shuo Zhou,† Feng-Lei Yang,* Xiaojun Wang, Xiguang Han*

Jiangsu Key Laboratory of Green Synthetic Chemistry for Functional Materials, School of Chemistry and Material Science, Jiangsu Normal University, Xuzhou, 221116 (P. R. China).

E-mail: yangfl@jsnu.edu.cn, xghan@jsnu.edu.cn

1. Experimental detail

1.1 Synthesis of MIL-68-In hexagonal micro-rods

In a typical synthesis, $In(NO_3)_3 \cdot 4H_2O$ (0.078 g, 0.21 mmol), terephthalic acid (0.021g, 0.18 mmol) were uniformly dissolved in 10 mL DMF. After stirring by ultrasonic concussion for 10 minutes, the mixture was transferred to a 50 mL Teflon-lined steel autoclave and placed in an oven at 100 °C for 4 hours. After reaction, the product was collected via centrifugation and washed several times with fresh ethanol, then dried at 60 °C overnight.

1.2 Preparation of MIL-68-In@In_2S_3

In a typical synthesis, In-MOF (0.5 g) and thioacetamide (TAA) (0.02 g, 0.266 mmol) were dissolved in 10 mL of methanol. After stirring by ultrasonic concussion for 10 minutes, the mixture was transferred to a 25 mL reaction kettle and placed in an oven at 150 ^{o}C for 4 hours. After this sulfidation reaction, the product was collected via centrifugation, washed several times with fresh ethanol, then dried at 60 °C overnight.

1.3 Preparation of *β*-In_2S_3/In_2O_3@N-C HHR

The *β*-In_2S_3/In_2O_3@N-C sample was synthesized via calcination of the obtained MOF@In_2S_3 at 500 °C for 2 h with heating rate of 5 °C·min^{-1} in the Ar atmosphere.

1.4 Preparation of In_2S_3@N-C.

The synthetic step of In_2S_3@N-C is the same as that of In_2O_3-In_2S_3@N-C, except that the amount of thioacetamide was 50 mg during the sulfidation process.

1.5 Preparation of In_2O_3@N-C.

The In_2O_3@N-C sample was synthesized via calcination of the obtained MIL-68-In hexagonal nanorods at 500 °C for 2 h with heating rate of 5 °C·min^{-1} in the Ar atmosphere.

1.6 Preparation of In_2O_3.

In_2O_3 structure was synthesized via calcination of the obtained MIL-68-In hexagonal nanorods at 500 °C for 2 h with heating rate of 5 °C·min^{-1} in the air atmosphere.

1.7 Characterization.

The composition and phase of the as-prepared products were acquired by the powder X-ray diffraction (XRD) pattern using a Panalytical X-pert diffractometer with CuKα radiation. The morphology and crystal structure of as-prepared products were

observed by scanning electron microscopy (SEM, SU8100), and high-resolution transmission electron microscopy (HRTEM, FEI Tecnai-F20) with an acceleration voltage of 200 kV. All TEM samples were prepared from depositing a drop of diluted suspensions in ethanol on a carbon film coated copper grid. PHI QUANTUM2000 photoelectron spectrometer (XPS) was using to characterize the surface compositions of product. The surface areas of these samples were measured by the Brunauer-Emmett-Teller (BET) method using nitrogen adsorption and desorption isotherms on a Micrometrics ASAP 2020 system.

1.8 Photocatalytic Activity Measurements.

For the selective oxidative coupling reaction of amine to imine, to a test tube, 0.025 mmol amine and 10 mg sample were separately dissolved into 2 mL acetonitrile. The result mixture was stirred under room temperature for a 36h under different light and then the catalyst was removed through centrifugation. The yield of the product was characterized by 1H NMR spectra. To perform the recycling experiments, the photocatalyst was recovered by centrifugation and washed with dichloromethane for several times. The recycled photocatalyst was then dried in vacuum at about 60 °C.

For the CDC reaction of indole and tetrahydroisoquinolin, the procedure was similar, but using 0.05 mmol tetrahydroisoquinolines and 0.1 mmol indoles instead of amine.

1.9 Photoelectrochemical measurements

Photoelectrochemical experiments were measured in the three electrode quartz cell, and catalyst-modified conductive glass (FTO, 25 cm^2) served as a working electrode, $Hg/HgCl_2$ electrode and platinum electrode were used as the reference electrode and

counter electrode, respectively. The catalyst ink was prepared by ultrasonically dispersing 10 mg of catalyst into a mixed solution containing 0.5 100 μL of the prepared catalyst ink was dropped onto the conductive glass and dried under room temperature. The conductive glass was then dried at 300 °C for 2 h. In the three electrode cell, added 0.025 M KH_2PO_4 and 0.025 M Na_2HPO_4 standard buffer as the electrolytes. The Linear Sweep Voltammetry（LSV), Amperometric i-t Curve(i-t） and A.C. Impedance（IMP）measurements were carried out on a CHI-760E workstation under 300W Xe arc lamp system was used as the visible-light irradiation source**.**

2.0 Density Functional Calculations

All of the density functional calculations were performed using plane-wave pseudopotential method, as implemented in the Quantum Espresso (QE) package Version 6.8 code [1, 2]. The generalized gradient approximation (GGA) with the Perdew–Burke–Ernzerhof (PBE) functional formulation[3] were used to describe the exchange-correlation effects. The ion-electron interaction was described by ultrasoft pseudopotential. A plane-wave kinetic energy cutoff of 500 eV was employed. Partial occupancies of electronic bands were allowed with the Gaussian smearing method with width of 0.01 eV. The self-consistent convergence accuracy was set at 1.0×10^{-5} eV/atom, and the convergence criterion for the force between atoms was 1.0×10^{-4} eV/Å. The K-Point mesh of 2 × 3 × 1 grid, featuring enough accuracy to total energy by convergence test, was used to sample the two-dimensional Brillouin zone for geometrical optimization of In_2S_3 (011) surface (In_2S_3-011) slab. The stoichiometric

In_2S_3-011 slab was separated by a >15 Å vacuum in Z direction. Based on various models, three-dimensional charge density difference of benzylamine adsorbed on In_2S_3-011 slab (benzylamine@In_2S_3-011) and projected density of state of (PDOS) of benzylamine, benzylamine@In_2S_3-011 and In_2S_3-011 have been conducted in this work. Moreover, The adsorption energy is typically evaluated as following formula: E_a = E(benzylamine@In_2S_3-011) – E(benzylamine) – E(In_2S_3-011), where E(benzylamine), E(In_2S_3-011) and E(benzylamine@In_2S_3-011) are single-point energy.

2. Experimental results

Fig. S1 XRD pattern of MIL-68-In hexagonal micro-rods precursor.

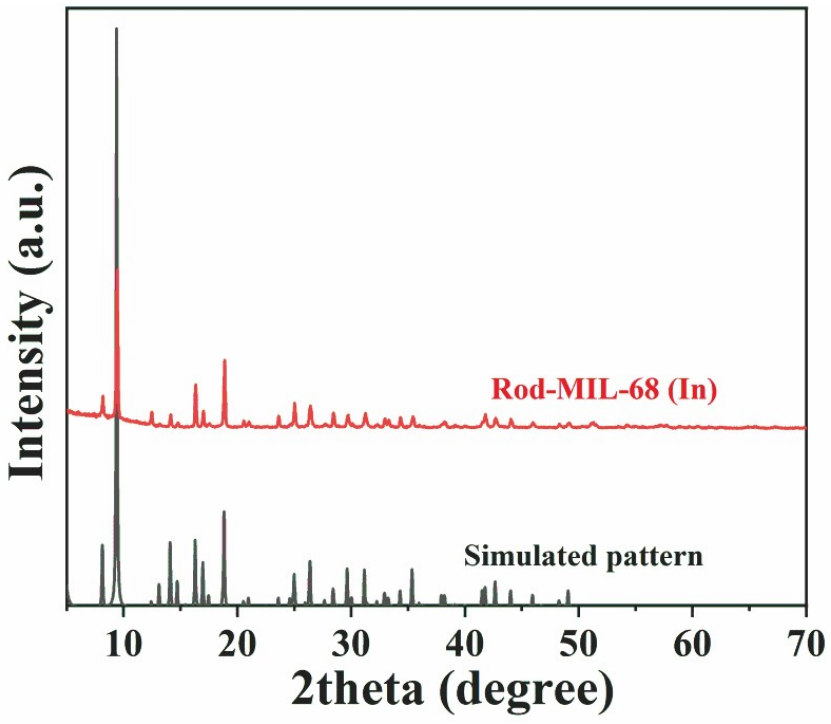

Fig. S2 (a) SEM image and (b-f) the corresponding element mapping of MIL-68-In micro-rods.

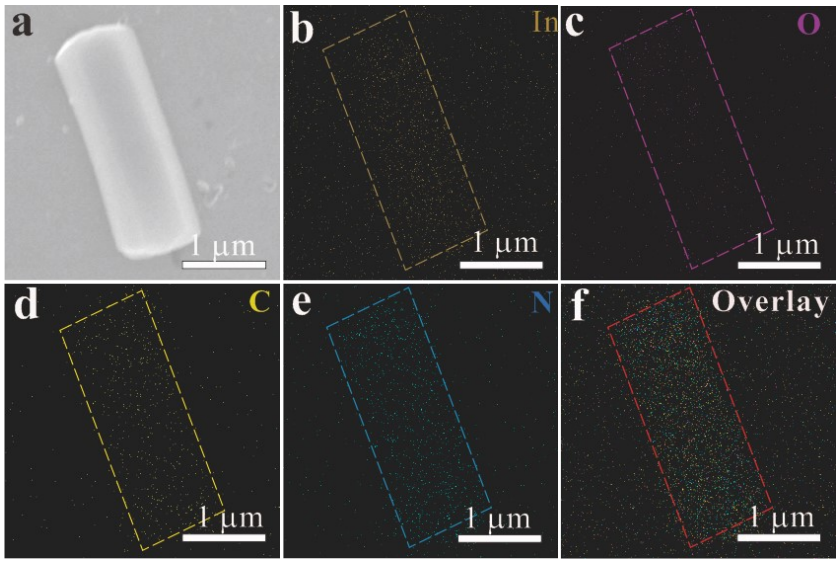

Fig. S3 XRD pattern of MIL-68-In after sulfidation (MIL-68-In@In_2S_3).

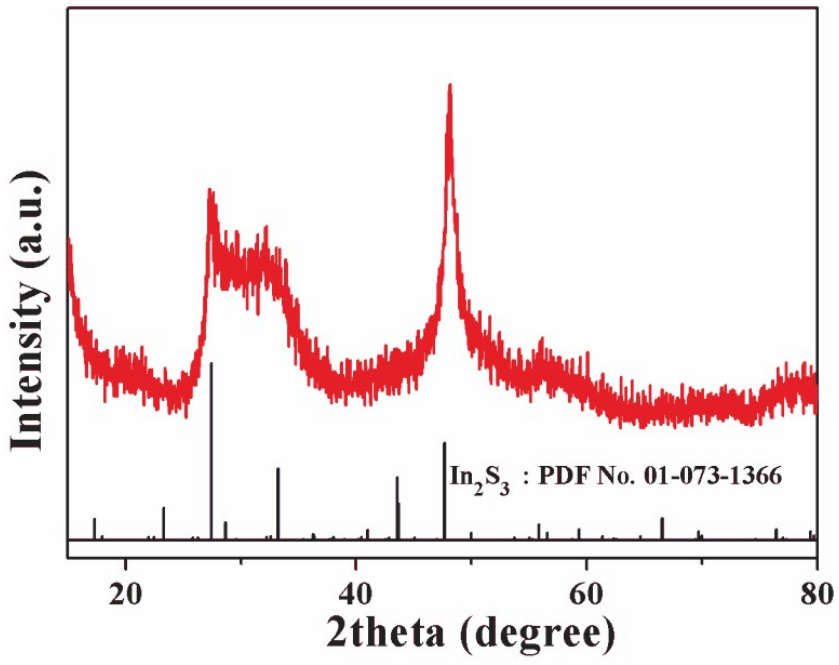

Fig. S4 TGA curves of the as-obtained MIL-68-In@In_2S_3.

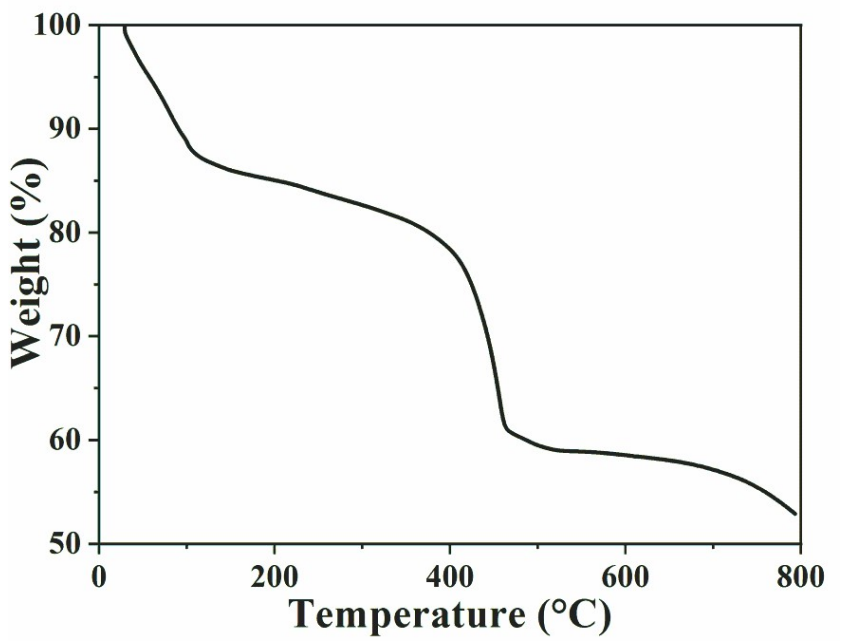

Table S1. Photocatalyzed oxidative amines to imines in different reaction conditions.

hυ (450 nm,LED)	Catalyst (β-In_2S_3/In_2O_3@N-C HHR)	Reaction time	Conv (%)
No	Yes	36 h	5%
Yes	No	36 h	9 %
Yes	Yes	36 h	97 %

Fig. S5 performance of β-In_2S_3/In_2O_3@N-C HHR in oxidative coupling of benzylamine under various light irradiation

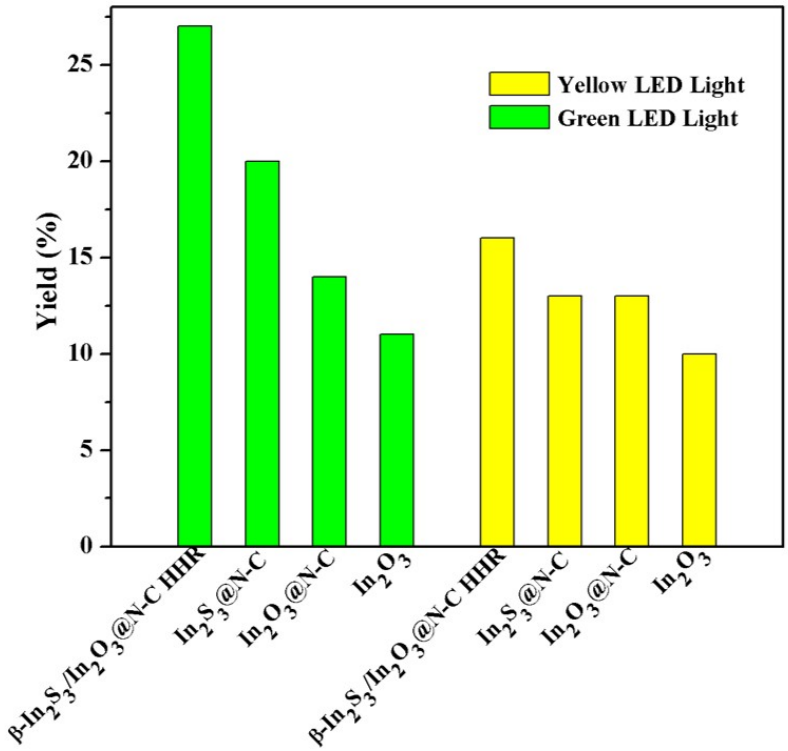

Fig. S6 (a) XRD pattern of In_2O_3@N-C, (b, c) SEM image of In_2O_3@N-C, (d-h) corresponding elemental mapping.

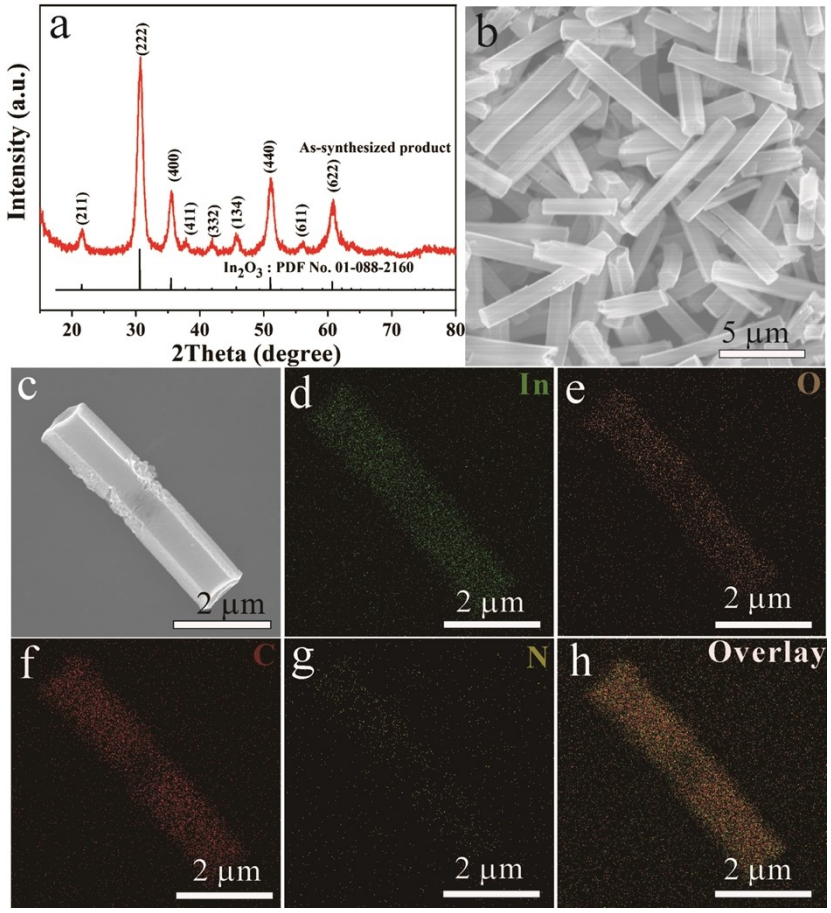

Fig. S7 (a) XRD pattern of In_2S_3@N-C, (b, c) SEM image of In_2S_3@N-C, (d-h) the corresponding elemental mapping.

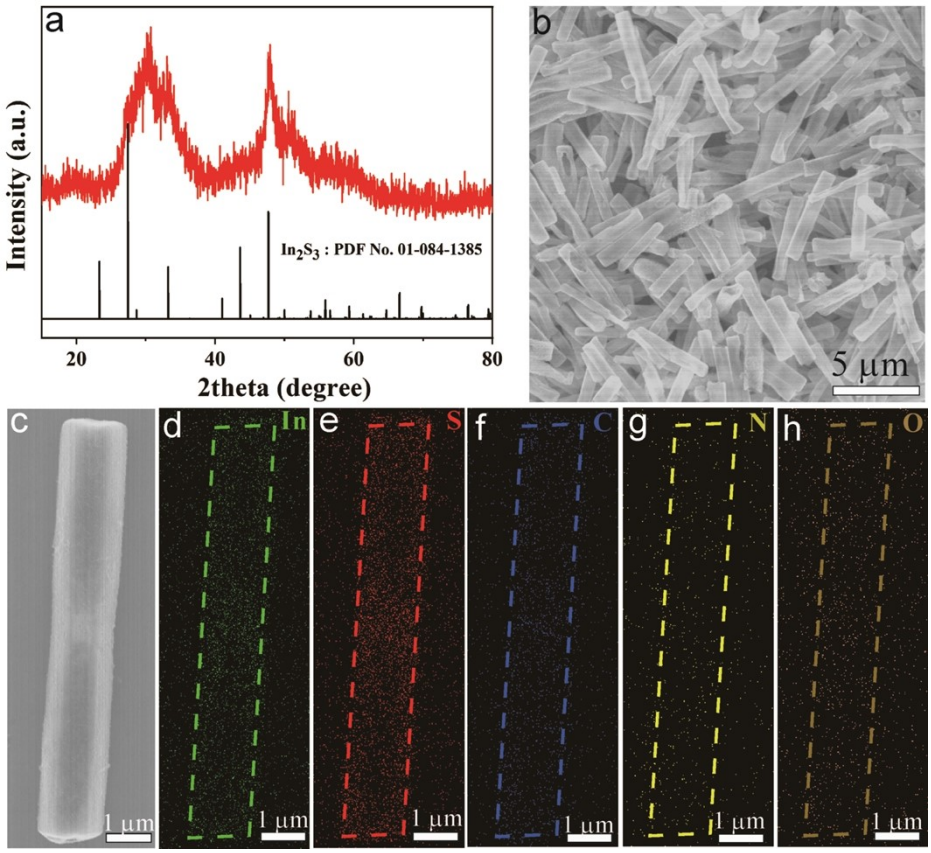

Fig. S8 (a) XRD pattern of In_2O_3, (b, c) SEM image of In_2O_3, (d-e) the corresponding elemental mapping.

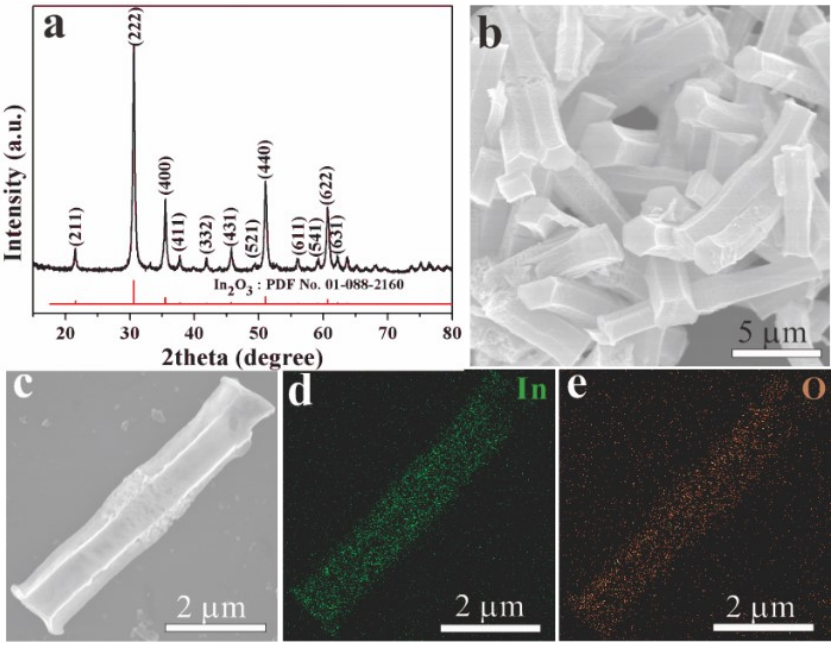

Fig. S9 (a) the curves of yield vs reacted time for oxidative coupling of benzylamine with β-In_2S_3/In_2O_3@N-C HHR, In_2S_3@N-C, In_2O_3@N-C and In_2O_3 as photocatalysts under blue light irradiation, (b) kinetic profiles of oxidative coupling of benzylamine using three catalysts under blue light irradiation.

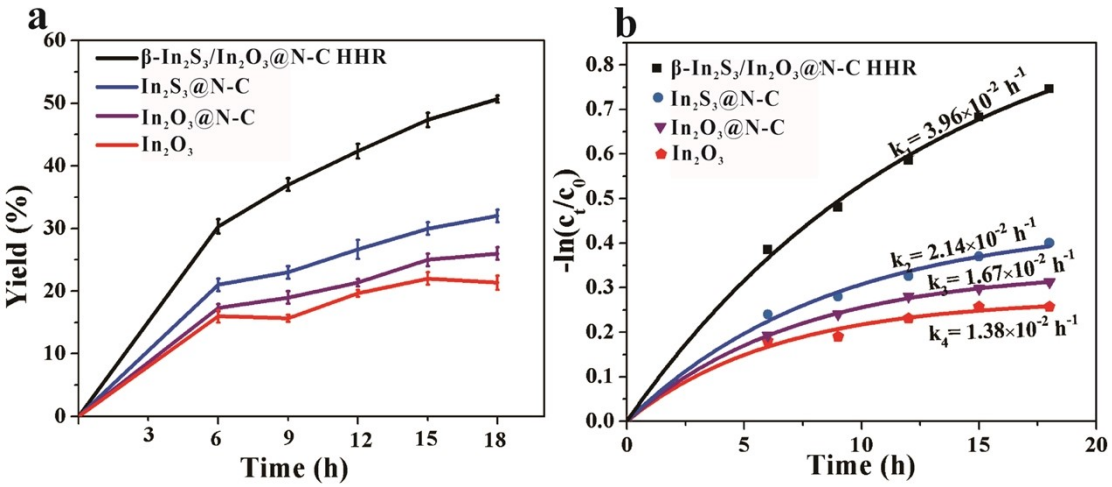

Fig. S10 (a) XRD pattern of β-In_2S_3/In_2O_3@N-C HHR after catalytic reaction, (b, c) SEM image of β-In_2S_3/In_2O_3@N-C HHR after catalytic reaction, (d-h) corresponding elemental mapping of β-In_2S_3/In_2O_3@N-C HHR after catalytic reaction.

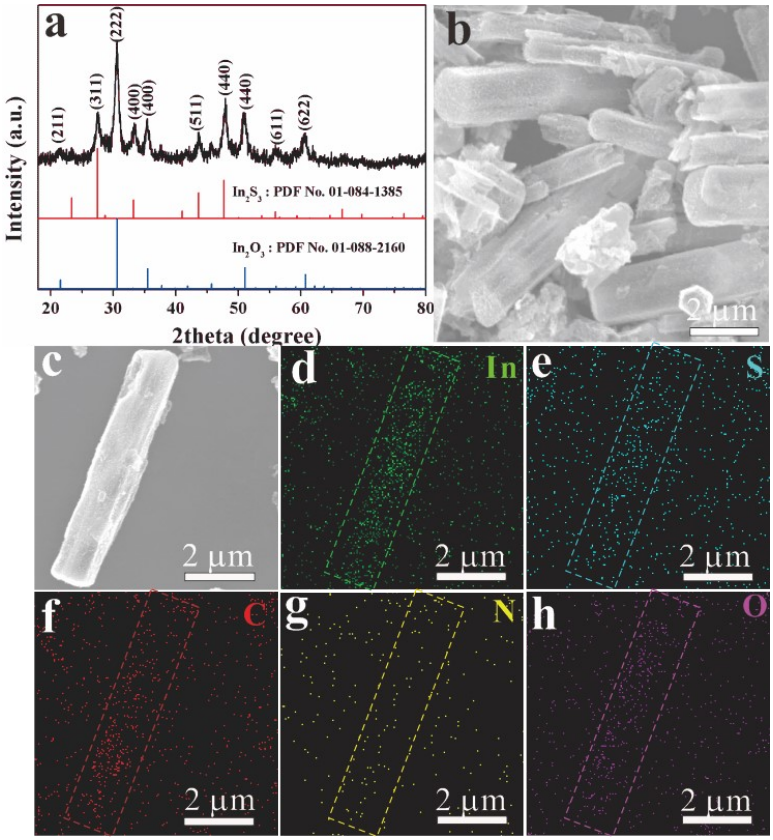

Fig. S11. (a) XRD pattern and (b) SEM image of *bulk*-In_2O_3.

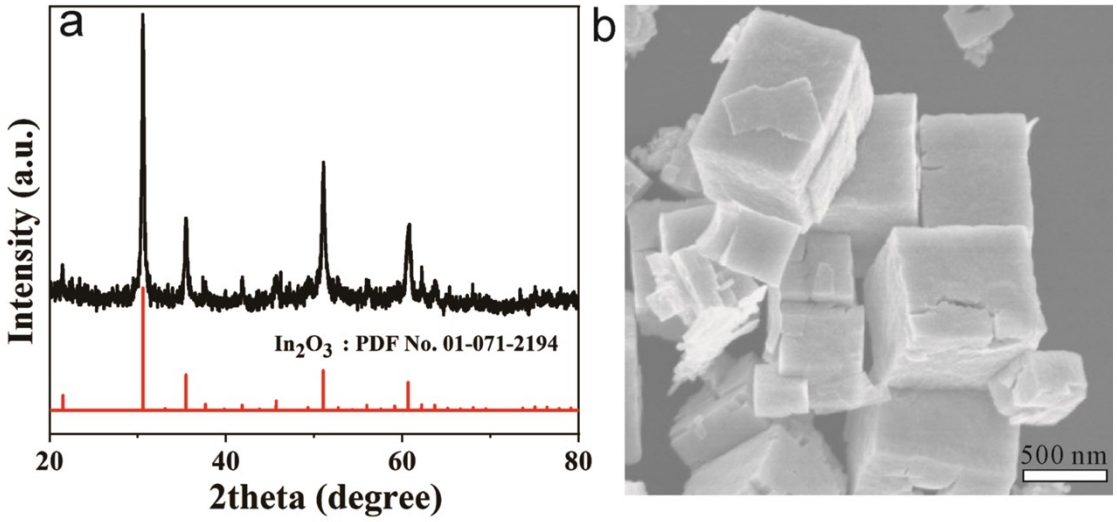

Fig. S12. (a) XRD pattern and (b) SEM image of tetragonal-β-In_2S_3.

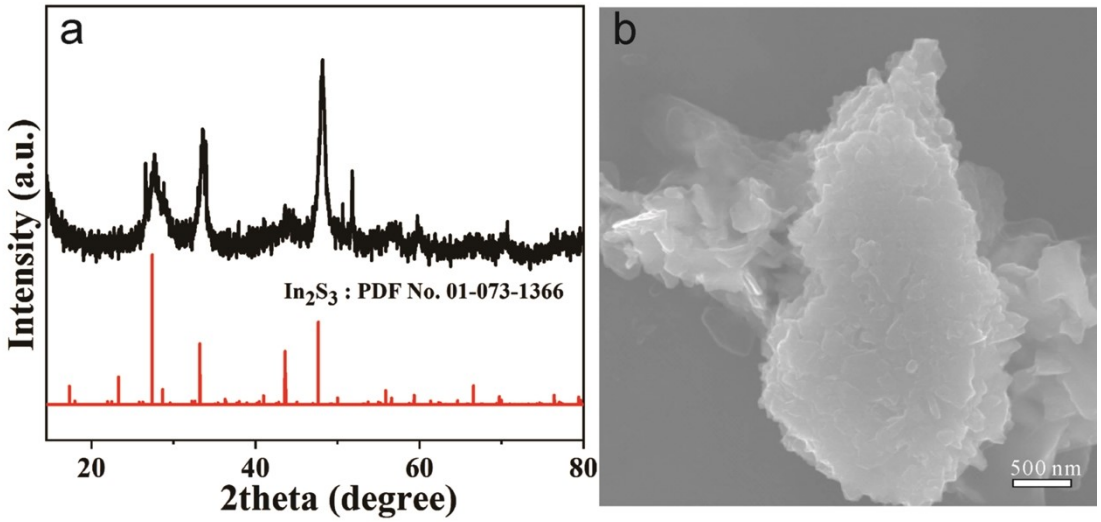

Fig. S13. Yields for oxidation of benzylamine to N-benzylidenebenzylamine with *β*-In_2S_3/In_2O_3@N-C HHR, In_2S_3@N-C, In_2S_3, In_2O_3@N-C, In_2O_3 and *bulk*-In_2O_3 as photocatalysts under blue light irradiation.

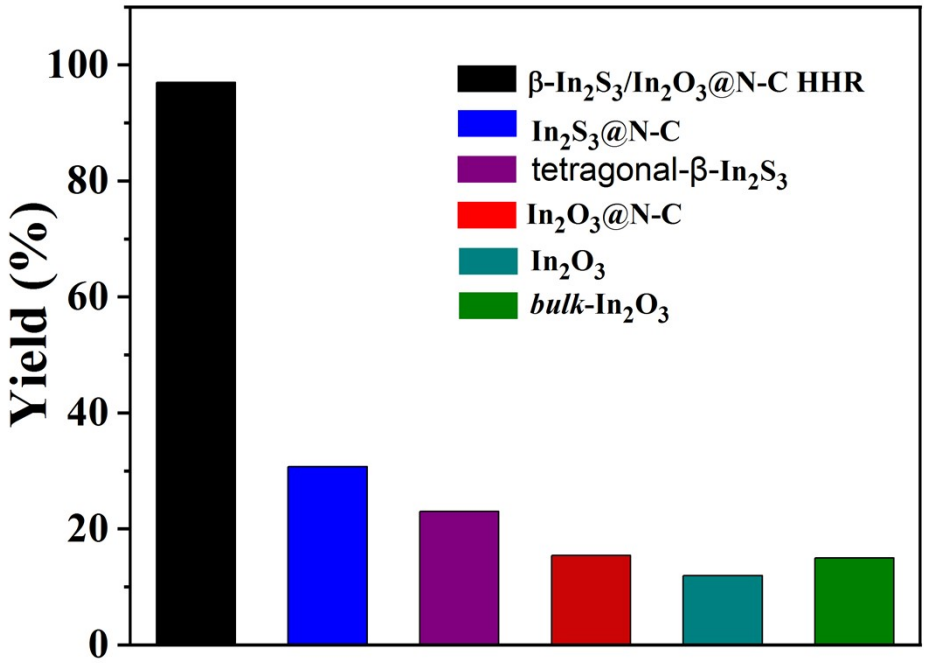

Fig. S14. TOF for oxidation of benzylamine to N-benzylidenebenzylamine with *β*-In_2S_3/In_2O_3@N-C HHR, In_2S_3@N-C, In_2O_3@N-C, and In_2O_3 as photocatalysts under blue light irradiation.

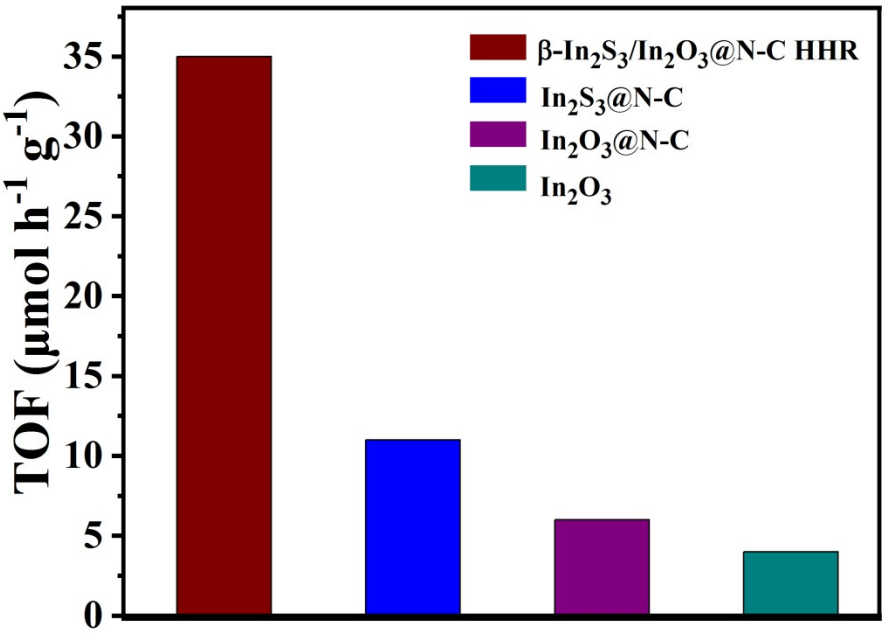

Fig. S15. Apparent quantum yield (AQY) of β-In_2S_3/In_2O_3@N-C HHR, In_2S_3@N-C, In_2O_3@N-C and In_2O_3.

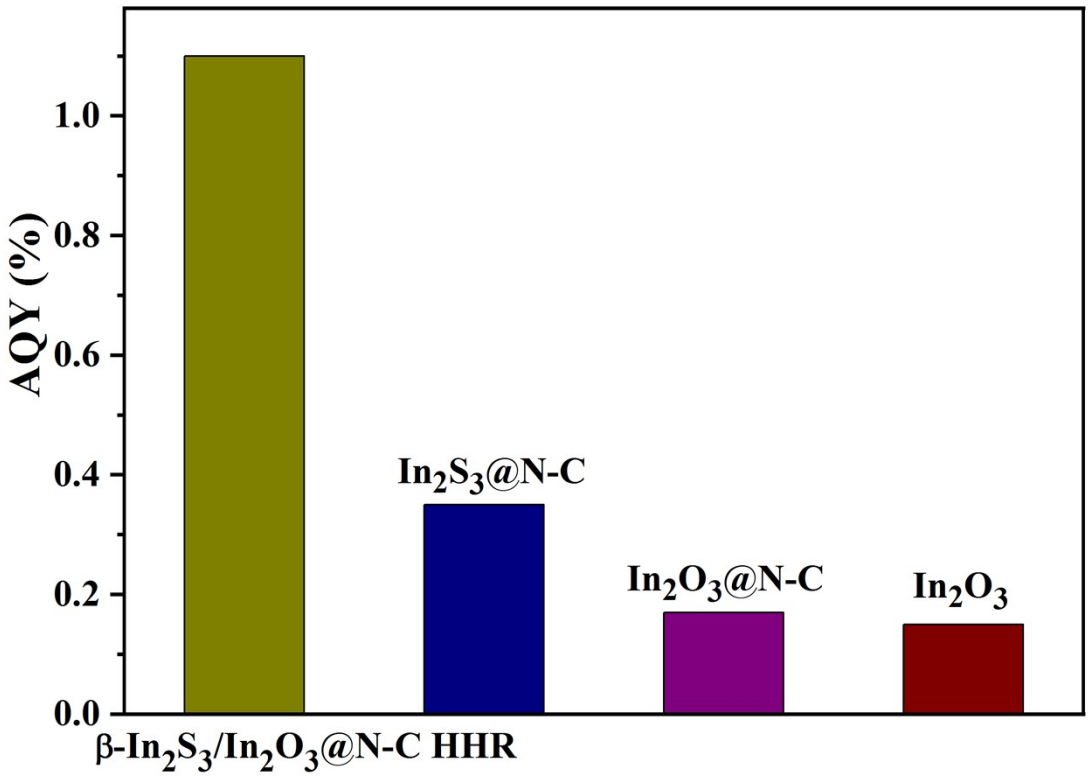

Fig. S16 Yields for CDC reaction of indole and tetrahydroisoquinoline with *β*-In_2S_3/In_2O_3@N-C HHR, In_2S_3@N-C, In_2O_3@N-C, and In_2O_3 as photocatalysts under blue light irradiation.

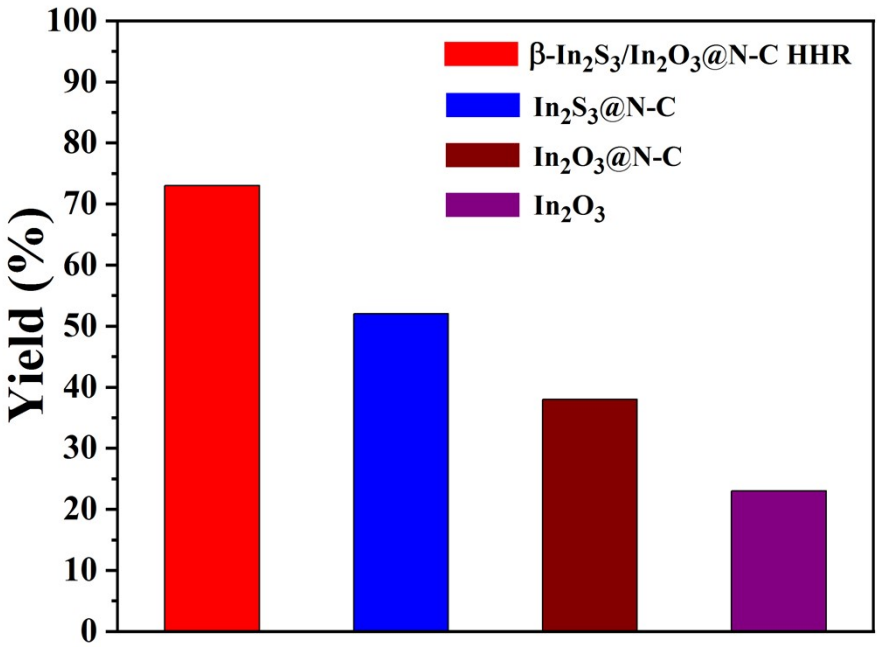

Fig. S17 UV-vis absorption spectra of β-In_2S_3/In_2O_3@N-C HHR, In_2S_3@N-C, In_2O_3@N-C and In_2O_3.

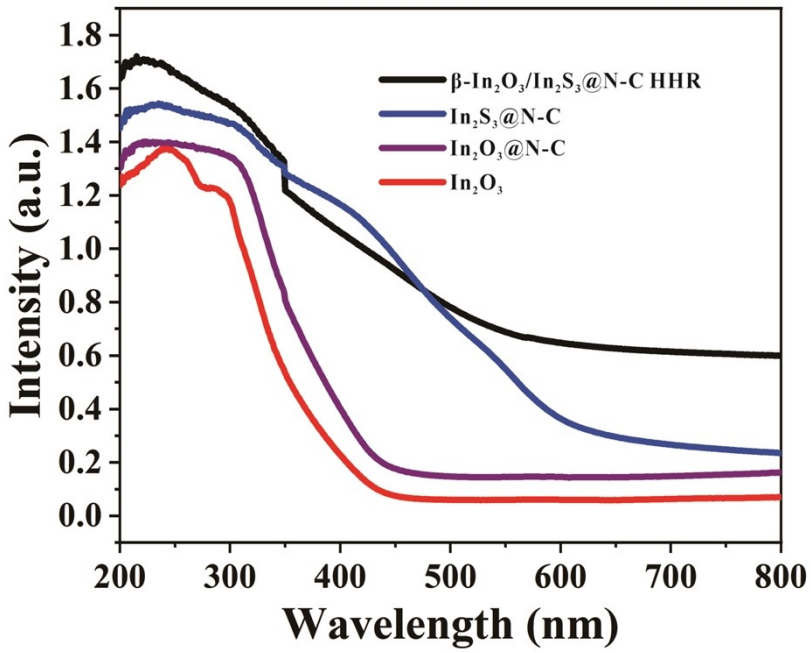

Fig. S18. Electron density difference maps of benzylamine (a): before adsorption (b) and after adsorption (c) on the In_2S_3-011 surface

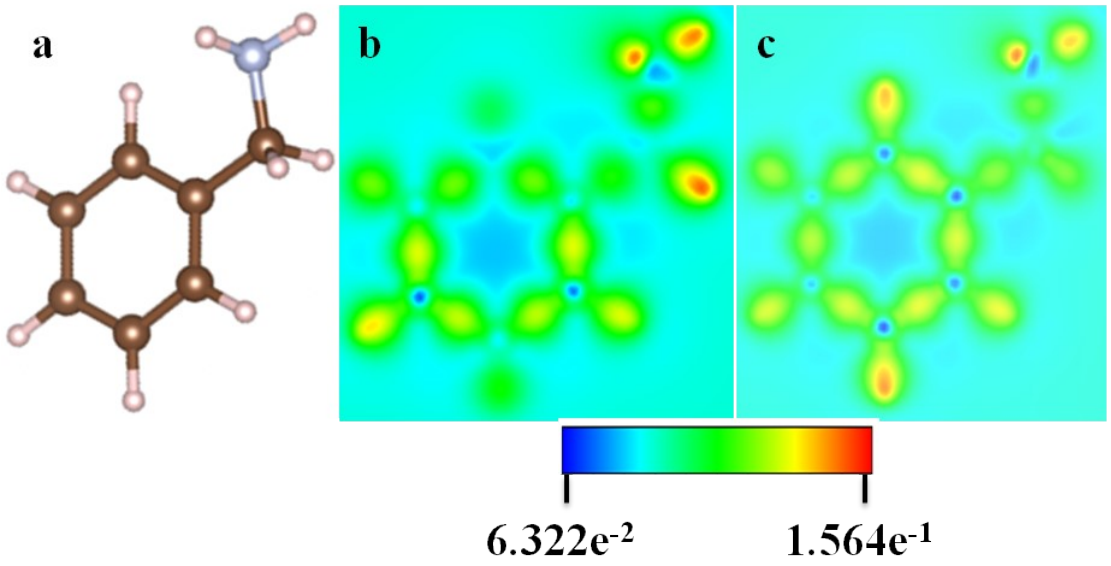

Fig. S19. Adsorption structure of benzylamine on In_2S_3-011 in the side view.

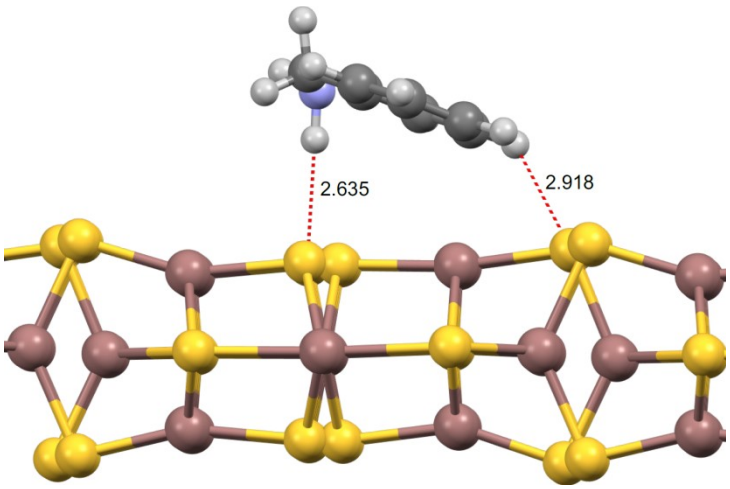

Fig. S20 (a) schematic showing the proposed reaction mechanism for oxidative coupling of amine to imine with β-In_2S_3/In_2O_3@N-C HHR as the photocatalyst, (b) control experiments for selective oxidation of amines to imines over β-In_2O_3/In_2S_3@N-C HHR coexistence with respective scavengers under blue LED irradiation, (c) UV–vis absorption spectra manifesting $TMPD^{\cdot+}$ using β-In_2S_3/In_2O_3@N-C HHR, In_2S_3@N-C, In_2O_3@N-C, In_2O_3 as catalysts.

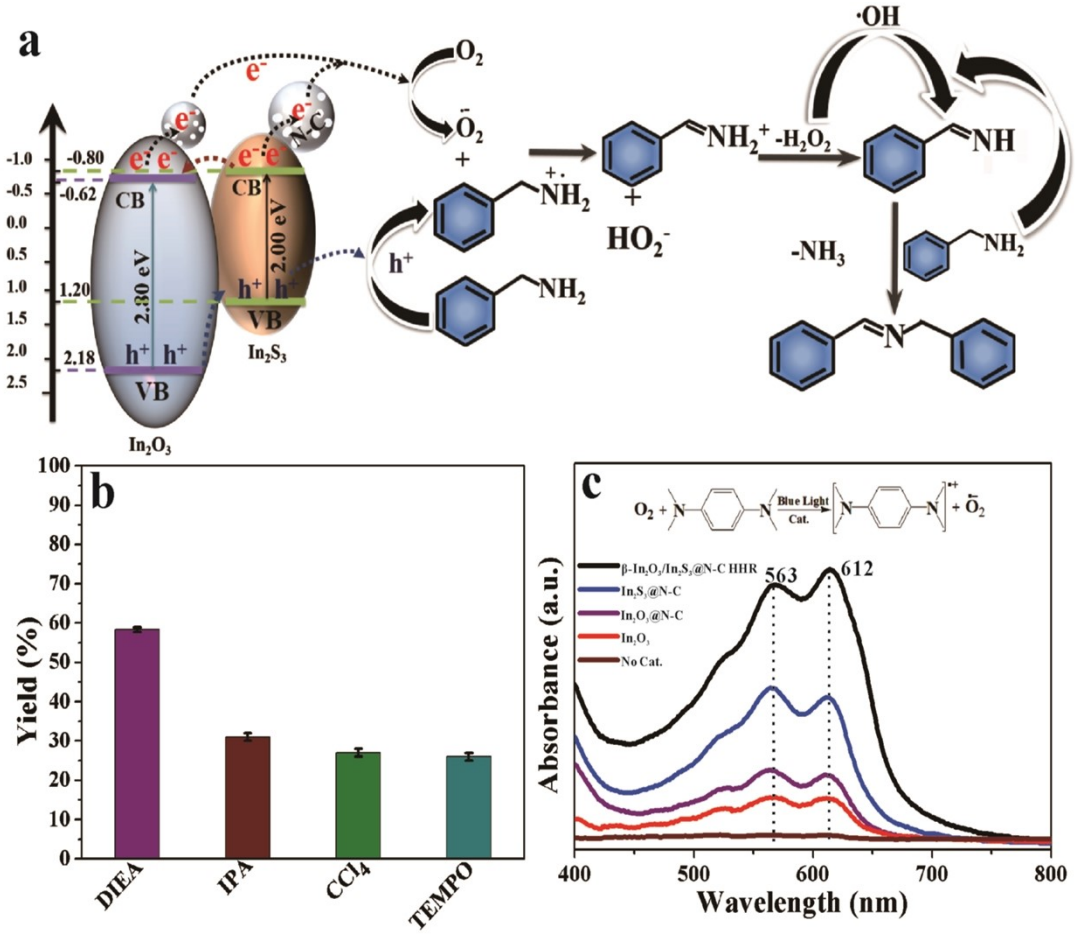

References

1 P. Giannozzi, O. Andreussi, T. Brumme, O. Bunau, M. Buongiorno Nardelli, M. Calandra, R. Car, C. Cavazzoni, D. Ceresoli, M. Cococcioni, N. Colonna, I. Carnimeo, A. Dal Corso, S. de Gironcoli, P. Delugas, R. A. DiStasio, A. Ferretti, A. Floris, G. Fratesi, G. Fugallo, R. Gebauer, U. Gerstmann, F. Giustino, T. Gorni, J. Jia, M. Kawamura, H. Y. Ko, A. Kokalj, E. Küçükbenli, M. Lazzeri, M. Marsili, N. Marzari, F. Mauri, N. L. Nguyen, H. V. Nguyen, A. Otero-de-la-Roza, L. Paulatto, S. Poncé, D. Rocca, R. Sabatini, B. Santra, M. Schlipf, A. P. Seitsonen, A. Smogunov, I. Timrov, T. Thonhauser, P. Umari, N. Vast, X. Wu and S. Baroni, *J. Phys.: Condens. Matter*, 2017, **29**, 465901.

2 P. Giannozzi, S. Baroni, N. Bonini, M. Calandra, R. Car, C. Cavazzoni, D. Ceresoli, G. L. Chiarotti, M. Cococcioni, I. Dabo, A. Dal Corso, S. de Gironcoli, S. Fabris, G. Fratesi, R. Gebauer, U. Gerstmann, C. Gougoussis, A. Kokalj, M. Lazzeri, L. Martin-Samos, N. Marzari, F. Mauri, R. Mazzarello, S. Paolini, A. Pasquarello, L. Paulatto, C. Sbraccia, S. Scandolo, G. Sclauzero, A. P. Seitsonen, A. Smogunov, P. Umari and R. M. Wentzcovitch, *J. Phys.: Condens. Matter*, 2009, **21**, 395502.

3 J. P. Perdew, K. Burke and M. Ernzerhof, *Phys. Rev. Lett.*, 1996, **77**, 3865-3868.